

# Universality classes of the Anderson transitions driven by quasiperiodic potential in the three-dimensional Wigner-Dyson symmetry classes

Xunlong Luo<sup>1,\*</sup> and Tomi Ohtsuki<sup>2,†</sup>

<sup>1</sup>*Science and Technology on Surface Physics and Chemistry Laboratory, Mianyang 621907, China*

<sup>2</sup>*Physics Division, Sophia University, Chiyoda-ku, Tokyo 102-8554, Japan*

(Dated: October 3, 2022)

Quasiperiodic system is an intermediate state between periodic and disordered systems with unique delocalization-localization transition driven by the quasiperiodic potential (QP). One of the intriguing questions is whether the universality class of the Anderson transition (AT) driven by QP is similar to that of the AT driven by the random potential in the same symmetry class. Here, we study the critical behavior of the ATs driven by QP in the three-dimensional (3D) Anderson model, Peierls phase model, and Ando model, which belong to the Wigner-Dyson symmetry classes. The localization length and two-terminal conductance have been calculated by the transfer matrix method, and we argue that their error estimations in statistics suffer from the correlation of QP. With the correlation under control, the critical exponents  $\nu$  of the ATs driven by QP are estimated by the finite size scaling analysis of conductance, which are consistent with  $\nu$ 's of the ATs driven by the random potential. Moreover, the critical conductance distribution and the level spacing ratio distribution have been studied. We also find that a convolutional neural network trained by the localized/delocalized wavefunctions in a disordered system predicts the localized/delocalized wavefunctions in quasiperiodic systems. Our numerical results strongly support that the universality classes of the ATs driven by QP and random potential are similar in the 3D Wigner-Dyson symmetry classes.

## I. INTRODUCTION

In the seminal work by Anderson, the extended wavefunction could become localized driven by random potential because of the quantum interference [1]. This delocalization-localization transition is called the Anderson transition (AT), which can be described by the single parameter scaling theory [2]. As a second-order phase transition, the universality class of AT, which is characterized by the critical exponents, depends on the symmetry and dimension, but not the detail of the system [3].

On the other hand, the quasiperiodic potential (QP) can also drive the Anderson localization, which has been extensively studied both theoretically [4–24] and experimentally [25–32]. Quasiperiodic systems are ubiquitous in nature and can be realized in the quasicrystals [33], photonic lattices [25–27], ultracold quantum gases [28–30, 34–37], and Moiré superlattices (i.e., the twisted bilayer graphene at 30° [38, 39]). One of the famous examples is the one-dimensional (1D) Aubry-André-Harper (AAH) model [4, 40], where there is a delocalization-localization transition with the same critical point at any Fermi energy due to the self-duality. Generalized AAH models involve the exact mobility edges [8–13], connections to higher-dimensional topological matter phases [41–45], and higher-dimensional ATs [17–20].

Both random potential and QP can drive the ATs, and a natural question is whether the universality classes of the ATs driven by QP and those by random potential

are the same or not [17]. For 1D and two-dimensional (2D) systems in orthogonal class, the infinitesimal random potential will localize the wavefunctions and there is no AT at all [2]. However, the 1D AAH model shows a delocalization-localization transition driven by QP with exact critical exponent  $\nu = 1$  [4], and the critical exponent is estimated as  $\nu \approx 1$  [19] for the generalized 2D AAH model. Both of them belong to the orthogonal class. Therefore the ATs in 1D and 2D AAH models belong to new universality classes without counterparts in the disordered systems. However, it is reported that the universality class of AT in the generalized three-dimensional (3D) AAH model is similar to that of the AT driven by random potential in 3D orthogonal class [17, 18]. Considering the uniqueness of 3D case, it is necessary to study the critical behavior by independent methods, such as the localization length, conductance, level statistics, and deep learning. Moreover, it is also interesting to check the conclusion in other symmetry classes, such as unitary and symplectic symmetry classes [46–48].

In this paper, we focus on the critical behavior of the ATs driven by QP in the 3D Anderson model (AM) [1], Peierls phase model (PPM) [49, 50], and Ando model [51, 52], which belong to orthogonal, unitary, and symplectic classes, respectively. The localization length and conductance have been calculated by the transfer matrix method [53–55]. We find that the estimates of their statistical error are difficult since the samples are not independent due to QP. Because the estimates of critical exponents  $\nu$  by the polynomial fitting method are sensitive to the error bar of the physical quantities [56], the incorrect error bar for the localization length or conductance will result in incorrect estimates of  $\nu$ . We have

\* luoxunlong@pku.edu.cn

† ohtsuki@sophia.ac.jp

TABLE I. Polynomial fitting results for the two-terminal conductance around the Anderson transition points for three dimensional Anderson model (AM), Peierls phase model (PPM) and Ando model with quasiperiodic potential. The goodness of fit (GOF), critical quasiperiodic potential strength  $V_c$ , critical exponent  $\nu$ , and the scaling dimension of the least irrelevant scaling variable  $-y$  are shown for various system sizes and for different orders of the Taylor expansion:  $(m_1, n_1, m_2, n_2)$ . The square bracket is the 95% confidence interval.

Model	$L$	$m_1$	$n_1$	$m_2$	$n_2$	GOF	$V_c$	$\nu$	$y$
AM	10-24	3	3	0	1	0.106	2.229[2.226, 2.233]	1.599[1.569, 1.637]	3.9[3.3, 4.6]
	10-28	3	3	0	1	0.101	2.233[2.230, 2.236]	1.613[1.587, 1.639]	3.5[3.0, 4.1]
PPM	10-24	3	3	0	1	0.105	2.335[2.331, 2.341]	1.43[1.39, 1.49]	3.0[2.2, 3.8]
	10-28	3	3	0	1	0.162	2.339[2.336, 2.342]	1.45[1.42, 1.49]	2.8[2.3, 3.4]
Ando	10-20	2	3	0	1	0.112	2.449[2.445, 2.455]	1.37[1.35, 1.39]	4.3[3.6, 4.9]
	10-20	3	3	0	1	0.139	2.449[2.445, 2.455]	1.36[1.34, 1.38]	4.3[3.7, 4.9]

chosen the proper number of samples so that they are regarded as independent, and the critical exponents  $\nu$  have been estimated based on the conductance, which are similar to those of the ATs driven by random potential (see Table I). Based on the critical points estimated by conductance, we also calculated the critical conductance distributions for the three models, which are independent of the system size and significantly different from each other. By properly taking account of the anisotropy, they are shown to be the same as those of disordered systems in the same symmetry class. Although the level spacing ratio distribution  $P(r)$  in the delocalized phase of 1D AAH model is special [57, 58], we find that  $P(r)$  in the delocalized states of the three models in this paper follow the Wigner-like surmises [59]. To further understand the localization properties, we constructed a convolutional neural network (CNN), whose parameters have been trained by the localized/delocalized wavefunctions in a disordered system [60]. We find this CNN can predict the localized/delocalized wavefunctions in quasiperiodic systems, which indicates that the localization properties in the disordered and quasiperiodic systems are similar.

The rest of the paper is organized as follows. In the next section, we will first introduce the three models with QP belonging to the Wigner-Dyson symmetry classes. Next, we will study the phase diagram spanned by eigenenergy and QP strength, and the mobility edge in section III. Then we will discuss the finite size scaling of conductance in section IV. Moreover, the critical conductance distribution (section V) and the level spacing ratio distribution (section VI) are studied. In section VII, we apply the CNN trained for the random potential to the wavefunctions in QP, and show that the CNN correctly predicts the critical strength of QP. The final section is devoted to the summary and concluding remarks.

## II. MODEL AND QUASIPERIODIC POTENTIAL

We first introduce the following tight-binding models defined on a 3D cubic lattice,

$$\mathcal{H} = \sum_{\mathbf{r}} \varepsilon_{\mathbf{r}} c_{\mathbf{r}}^{\dagger} c_{\mathbf{r}} + \sum_{\langle \mathbf{r}, \mathbf{r}' \rangle} e^{2\pi i \theta_{\mathbf{r}, \mathbf{r}'}} c_{\mathbf{r}}^{\dagger} c_{\mathbf{r}'}, \quad (1)$$

where  $c_{\mathbf{r}}^{\dagger}$  ( $c_{\mathbf{r}}$ ) is the creation (annihilation) operator.  $\mathbf{r}$  and  $\mathbf{r}'$  specify the cubic lattice site;  $\mathbf{r} = (r_x, r_y, r_z)$  and  $r_{\mu} = 1, 2, \dots, L_{\mu}$  with  $\mu = x, y, z$ .  $\langle \mathbf{r}, \mathbf{r}' \rangle$  means that  $\mathbf{r}$  and  $\mathbf{r}'$  are the nearest neighbor lattice sites.  $i = \sqrt{-1}$  is the imaginary unit. The model in Eq. (1) is the Anderson model with  $\theta_{\mathbf{r}, \mathbf{r}'} = 0$  [1]. When  $\theta_{\mathbf{r}, \mathbf{r} + \mathbf{e}_z} = \Phi r_x$  with  $\mathbf{e}_z$  the unit vector in  $z$  direction and  $\theta_{\mathbf{r}, \mathbf{r}'} = 0$  in the hoppings along  $x$  and  $y$  directions, the model is the Peierls phase model [49, 50].  $\Phi$  is a magnetic gauge flux that penetrates through every square plaquette in the  $z$ - $x$  plane of the cubic lattice in units of  $h/e$ , where  $h$  is the Planck constant and  $e$  is the elementary charge. We set  $\Phi = 0.1$  in the following calculations.

The Ando model can be constructed in the 3D cubic lattice as follows [51, 52],

$$\mathcal{H} = \sum_{\mathbf{r}} \varepsilon_{\mathbf{r}} c_{\mathbf{r}, \sigma}^{\dagger} c_{\mathbf{r}, \sigma} + \sum_{\langle \mathbf{r}, \mathbf{r}' \rangle, \sigma, \sigma'} R(\mathbf{r}, \mathbf{r}')_{\sigma, \sigma'} c_{\mathbf{r}, \sigma}^{\dagger} c_{\mathbf{r}', \sigma'}, \quad (2)$$

where  $c_{\mathbf{r}, \sigma}^{\dagger}$  ( $c_{\mathbf{r}, \sigma}$ ) is the creation (annihilation) operator with  $\sigma = \uparrow, \downarrow$ . We set the spin-orbit coupling between the nearest neighbor lattice sites as  $R(\mathbf{r}, \mathbf{r} + \mathbf{e}_{\mu}) = e^{i\theta \sigma_{\mu}}$ , where  $\mathbf{e}_{\mu}$  is the unit vector in the  $\mu = x, y, z$  directions and  $\sigma_{\mu}$  is the Pauli spin matrix. The parameter  $\theta$ , which is set to be  $\theta = \pi/6$  in our simulations, represents the strength of spin-orbit coupling.

$\varepsilon_{\mathbf{r}}$  in Eq. (1) and (2) is the onsite potential. Here we study the critical behavior of ATs driven by QP, so the QP is added into these three models instead of random potential. QP has already been directly realized in the photonic lattices [25, 26], ultracold atomic experiments [28–30, 34–37], and Moiré superlattices [38, 39]. Following Ref. 17, we set

$$\varepsilon_{\mathbf{r}} = 2V \sum_{i=1}^3 \cos(2\pi \mathbf{b}_i \cdot \mathbf{r} + \phi_i), \quad (3)$$

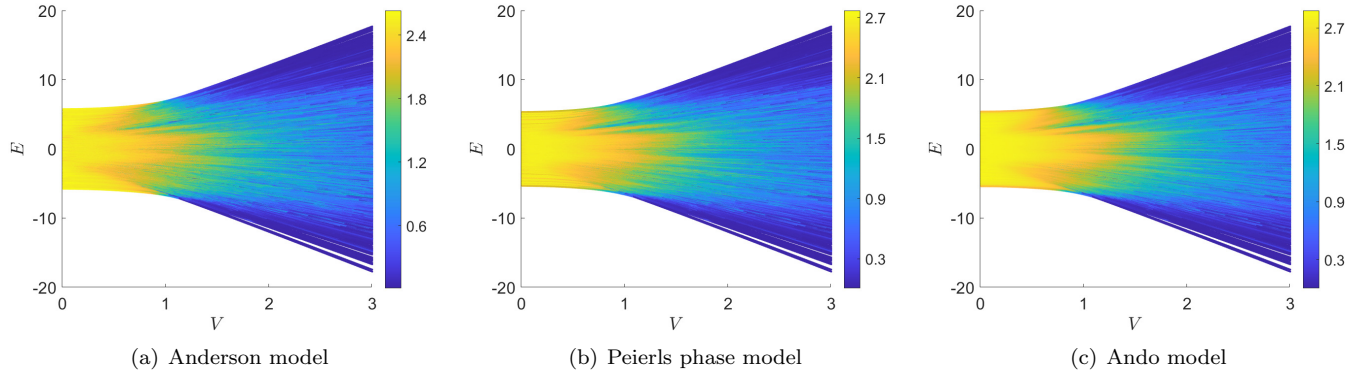


FIG. 1. Normalized participation ratio in the logarithmic form  $\eta$  for different eigenenergies  $E$  as a function of quasiperiodic potential strength  $V$  for the three quasiperiodic models.  $\eta \approx 3$  stands for the well delocalized state and  $\eta \approx 0$  for the strongly localized state.  $\eta$  is simulated with cubic system with linear size  $L = 10$ .

where  $V$  is the strength of QP,  $\{\mathbf{b}_i\}$  are vectors determining the quasiperiodicity, and  $\{\phi_i\}$  are the arbitrary phases. We write  $\mathbf{b}_i$  in the matrix form  $\mathbf{B} = [\mathbf{b}_1 \ \mathbf{b}_2 \ \mathbf{b}_3]^T$ . In order to keep quasiperiodicity and make the model nonseparable, we set  $\mathbf{B} = \beta \mathbf{R}(\alpha)$  with  $\beta = \frac{\sqrt{5}-1}{2}$  and

$$\mathbf{R}(\alpha) = \begin{bmatrix} c^2 + s^3 & cs & cs^2 - cs \\ cs & -s & c^2 \\ cs^2 - cs & c^2 & c^2 s + s^2 \end{bmatrix}, \quad (4)$$

where  $c = \cos(\alpha)$  and  $s = \sin(\alpha)$ .  $\beta = \frac{\sqrt{5}-1}{2}$  is the golden mean, which is an irrational number characterizing the quasiperiodicity.  $\mathbf{R}(\alpha)$  is a symmetric orthonormal matrix which makes the model nonseparable, as long as we avoid  $\alpha = 0$ ,  $\alpha = \pi/2$ , and multiples thereof. In the following calculations, we set  $\alpha = \pi/7$ . We always impose open boundary condition in the calculations because of the quasiperiodicity. In order to simulate many samples, we randomize the arbitrary phases  $\{\phi_i\}$  in the cosines within  $(0, 2\pi]$ . These systems will be equivalent by an overall translation in the thermodynamic limit.

### III. PHASE DIAGRAM AND MOBILITY EDGE

We first study the phase diagrams of these models spanned by the eigenenergy  $E$  and the QP strength  $V$ . Here, we diagonalize the Hamiltonians in cubic systems with linear size  $L$  and obtain the eigenenergies  $\{E_i\}$  and the normalized eigenfunctions  $\{\psi_i(\mathbf{r})\}$ . The participation ratio for the eigenfunction  $\psi_i(\mathbf{r})$  is defined as

$$\text{PR}(E_i) \equiv \frac{1}{\sum_{\mathbf{r}} |\psi_i(\mathbf{r})|^4}. \quad (5)$$

The delocalization/localization states can be characterized by the normalized participation ratio [13, 61, 62] in the logarithmic form, which is defined as

$$\eta(E_i) \equiv \frac{\ln \text{PR}(E_i)}{\ln L}. \quad (6)$$

When the wavefunction is well delocalized,  $\text{PR} \sim L^3$  and  $\eta \approx 3$ . On the contrary, when the wavefunction is localized,  $\text{PR} \sim \xi^3$  with  $\xi$  the localization length, and  $\eta \approx 0$ .  $\eta$  is plotted in the plane spanned by  $E$  and  $V$  (Fig. 1) for the three quasiperiodic models introduced in Section II. As seen in Fig. 1, the values of  $\eta$  change rapidly, indicating the existence of mobility edges which fluctuate significantly as we vary QP strength  $V$ .

From now we focus on the Fermi energy level  $E = 0$  and analyze the critical behavior. In order to characterize the delocalization-localization transitions, the localization length and conductance are calculated by the transfer matrix method. Then the critical exponents are extracted by the polynomial fitting method. We note that the fitting is sensitive to the statistical error estimates of the fitting data, and the incorrect error estimates result in incorrect evaluation of critical exponents. Therefore we should be careful of the statistical error estimates of the localization length and conductance in quasiperiodic systems. We argue that there is a correlation between samples for localization length and conductance resulting from the QP, which result in incorrect error estimates of them. However, the correlation can be controlled by the limited number of samples (see the detailed analysis in Appendices B and C). In this paper, we take conductance as an example to study the critical behavior. We think the localization length analysis also gives a similar result if the error estimates are correctly done.

In the next section, we will introduce the calculation of conductance and perform the finite size scaling analysis to extract the critical parameters, such as critical exponent  $\nu$  and critical quasiperiodic potential strength  $V_c$ .

#### IV. FINITE SIZE SCALING OF THE CONDUCTANCE

The zero temperature two-terminal conductance in units of  $e^2/h$  is given by

$$g = \text{tr}(tt^\dagger) \quad (7)$$

with  $t$  the transmission matrix. The transmission matrix  $t$  can be calculated by the transfer matrix method [63]. The two-terminal conductance is calculated along  $z$  direction with ideal lead in the two side of the cubic system ( $L_x = L_y = L_z = L$ ).

The mean conductance  $\langle g \rangle$  is averaged over 50000 samples for the AM and PPM,  $10^5$  samples for the Ando model with random phase  $\{\phi_i\}$ . We note that  $g(\{\phi_i\})$  and  $g(\{\phi_i + \delta\phi_i\})$  are correlated for small  $\delta\phi_i$ , but uncorrelated when  $\delta\phi_i$  is large enough (see Appendix B), just like the magnetoconductance in mesoscopic systems [64–68]. The behavior of the mean conductance  $\langle g \rangle$  or logarithmic average  $\langle \ln g \rangle$  with error bar are shown in Fig. 2 for various  $V$  and  $L$ . The scale invariant point of conductance indicates the critical point  $V_c$  of the AT driven by QP. With  $V < V_c$  ( $V > V_c$ ), the conductance increases (decreases) with system size  $L$ , indicating it is in the delocalized (localized) phase. To extract the universal critical parameters near the critical point, the polynomial fitting method based on the finite size scaling theory is introduced as follows.

The single parameter scaling theory [2] assumes that the dimensionless physical quantity  $\Gamma$ , such as the normalized localization length and the two-terminal conductance, obeys the universal scaling function,

$$\Gamma = f(\phi_1 L^{1/\nu}), \quad (8)$$

where  $\phi_1$  is the relevant scaling variable,  $L$  is the system size, and  $\nu$  is the critical exponent describing the power-law divergence of the length scales near the critical point. For the actual fitting, we often need to take into account the irrelevant scaling variables because of the corrections to the single parameter scaling [56, 69]. Here we just consider the least-irrelevant scaling variable  $\phi_2$ , then the universal scaling function can be written as

$$\Gamma = F(\phi_1 L^{1/\nu}, \phi_2 L^{-y}), \quad (9)$$

where  $-y$  is the scaling dimension for the irrelevant scaling variable. The term  $\phi_2 L^{-y}$  will decrease to zero in power-law with  $L$  increasing and the scaling function returns to the single parameter scaling form in Eq. (8) in the thermodynamic limit. The relevant or irrelevant scaling variables depend on the system parameter driving the AT. In this paper, QP strength  $V$  is this system parameter, and a normalized distance of  $V$  from the critical point  $V_c$  is define as  $w \equiv (V - V_c)/V_c$ . Then scaling variables  $\phi_1$  and  $\phi_2$  are functions of  $w$  with  $\phi_1(w = 0) = 0$  by definition. Considering the possible non-linearity of  $w$  near the critical point,  $\phi_1$  and  $\phi_2$  are expanded in powers

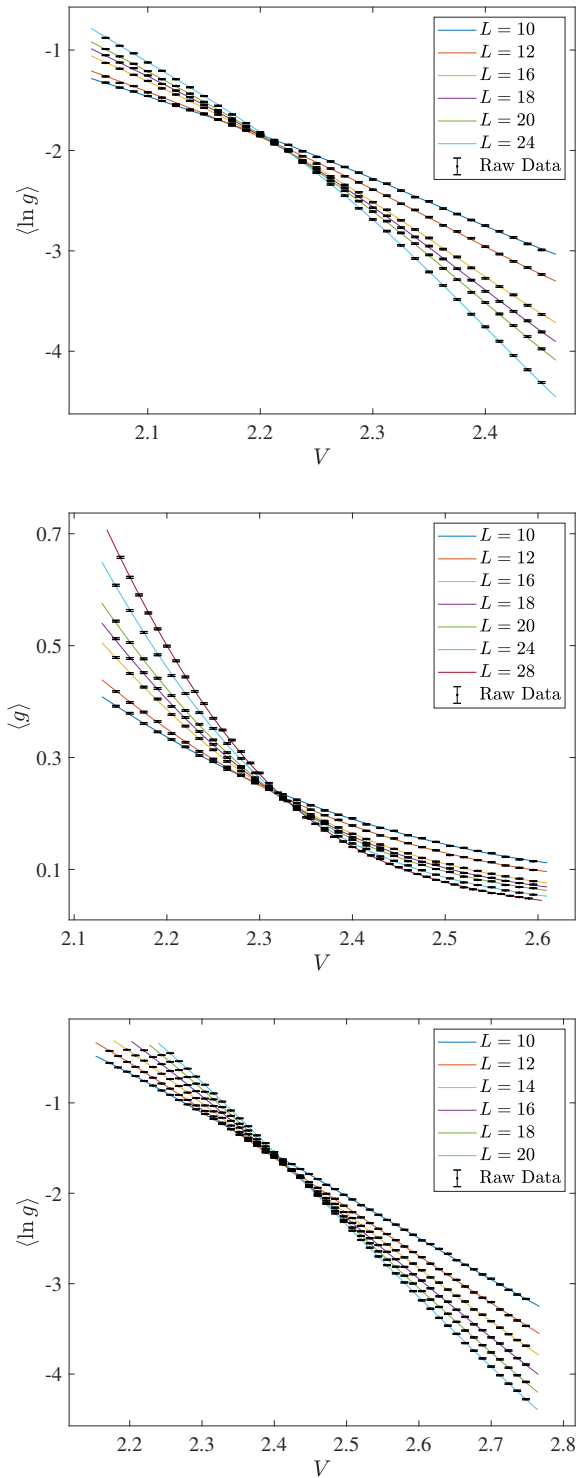


FIG. 2. The two-terminal conductance as a function of the strength of quasiperiodic potential  $V$  for Anderson, Peierls phase, and Ando models (from top to bottom). The black points with the error bars are the raw data and lines with different colors are the polynomial fitting results with expansion order  $(m_1, n_1, m_1, n_1) = (3, 3, 0, 1)$ .

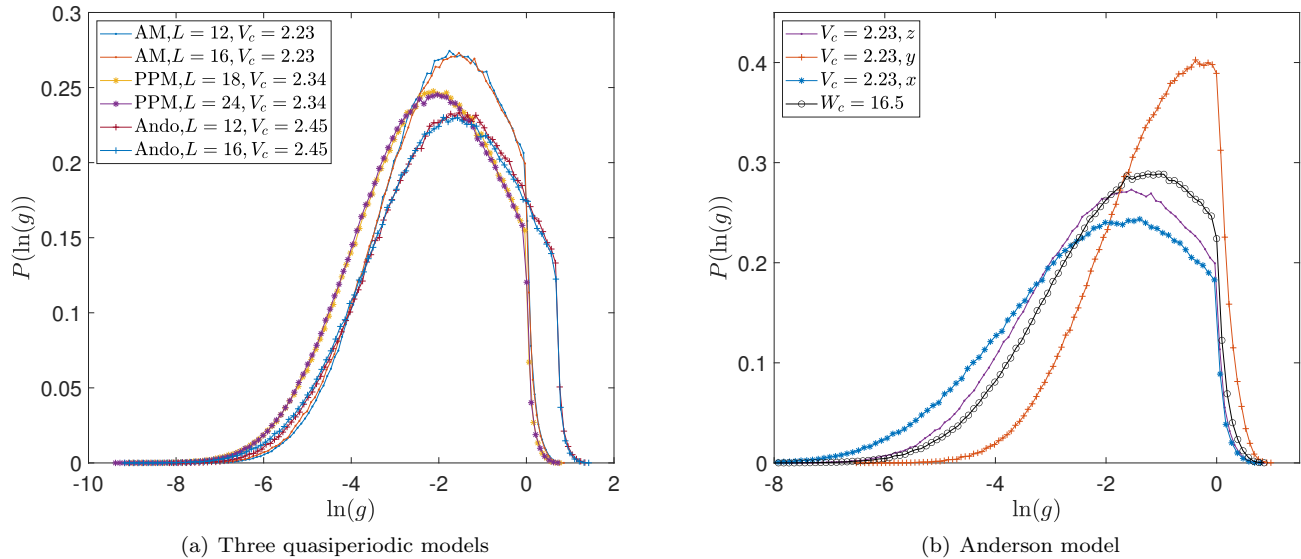


FIG. 3. (a) Critical conductance distributions (CCDs) along  $z$  direction for the Anderson model (AM), Peierls phase model (PPM), and Ando model at critical quasiperiodic potential  $V_c$  estimated in TABLE I. (b) The CCDs of quasiperiodic AM along  $x$ ,  $y$ , and  $z$  directions. For comparison, the CCD of disordered AM at critical disorder  $W_c$  is also shown in circles. The two-terminal conductance  $g$  is calculated in cubic system with linear size  $L$  and  $L = 16$  for (b). Data for each distribution comes from  $10^6$  samples.

of small  $w$  when  $V$  is sufficiently close to  $V_c$ ;

$$\phi_i(w) \equiv \sum_{j=0}^{m_i} b_{i,j} w^j \quad (10)$$

with  $i = 1, 2$ ,  $b_{1,0} = 0$ . When  $V$  is sufficiently close to  $V_c$  and the values of  $\Gamma$  are controlled in a finite range, the universal scaling function  $F$  in Eq. (9) can also be expanded in powers of its small arguments,

$$F = \sum_{j_1=0}^{n_1} \sum_{j_2=0}^{n_2} a_{j_1, j_2} (\phi_1 L^{1/\nu})^{j_1} (\phi_2 L^{-y})^{j_2}. \quad (11)$$

To reduce the redundant two degrees of freedom in Eq. (11), we set  $a_{0,1} = a_{1,0} = 1$ . We note that the assumption here is a posteriori justified by the numerical analysis.

Given  $(m_1, n_1, m_2, n_2)$  in Eqs. (10) and (11),  $F$  is a finite-order of polynomial of  $L$  and  $w \equiv (V - V_c)/V_c$ . Numerical data of  $\Gamma$  for different  $L$  and  $V$  are fitted by the polynomial with fitting parameters  $V_c$ ,  $\nu$ ,  $y$ ,  $a_{i,j}$  and  $b_{i,j}$ . We minimize  $\chi^2$  in terms of the fitting parameters,

$$\chi^2 \equiv \sum_{k=1}^{N_D} \frac{(\Gamma_k - F_k)^2}{\sigma_{\Gamma_k}^2}. \quad (12)$$

Here  $k$  counts the data points ( $k = 1, \dots, N_D$ ), and each data point is specified by  $L$  and  $V$ ;  $k = (L, V)$ .  $\Gamma_k$  and  $\sigma_{\Gamma_k}$  are a mean value of dimensionless physical quantity and its standard deviation at  $k = (L, V)$ , respectively, while  $F_k$  is the fitting value from the polynomial  $F$  at

$k = (L, V)$ .  $F_k$  depends on the fitting parameters and  $\chi^2$  is minimized in terms of them. The minimization is carried out for several different choices of  $(m_1, n_1, m_2, n_2)$ . The quality of the fitting is characterized by the goodness of fit in statistics [70, 71]. The 95% confidence intervals for the fitting results are determined by 1000 sets of  $N_D$  synthetic data points, which are statistically generated from the fitting value  $F_k$  with the same standard deviation of  $\Gamma_k$  at each point  $k$ .

Here the dimensionless physical quantity conductance [ $\langle g \rangle$  or  $\langle \ln g \rangle$ ] will be fitted by the polynomial fitting method. The fitting results with the goodness of fit greater than 0.1 are shown in Table I.  $V_c$  and  $\nu$  are shown to be robust against the change of the expansion orders and various system sizes in Table I. The critical exponents  $\nu$  are estimated as  $\nu = 1.613$  [1.587, 1.639] for the AM,  $\nu = 1.45$  [1.42, 1.49] for the PPM, and  $\nu = 1.37$  [1.35, 1.39] for the Ando model, which are consistent with the critical exponents of ATs driven by random potential, i.e.,  $\nu \approx 1.57$  [56] for 3D orthogonal class,  $\nu \approx 1.43$  [69] for 3D unitary class, and  $\nu \approx 1.36$  [72] for 3D symplectic class, respectively. We also find that the critical QP strength  $V_c$  increases for the PPM and Ando model compared with that for the AM, which is similar to that in disordered systems. This increase of  $V_c$  by the magnetic field (Peierls phase model) and spin-orbit interaction (Ando model) is consistent with the weak localization [73]. In conclusion, the universality classes of ATs driven by QP are similar to those of ATs driven by the random potential in the 3D Wigner-Dyson symmetry classes [17].

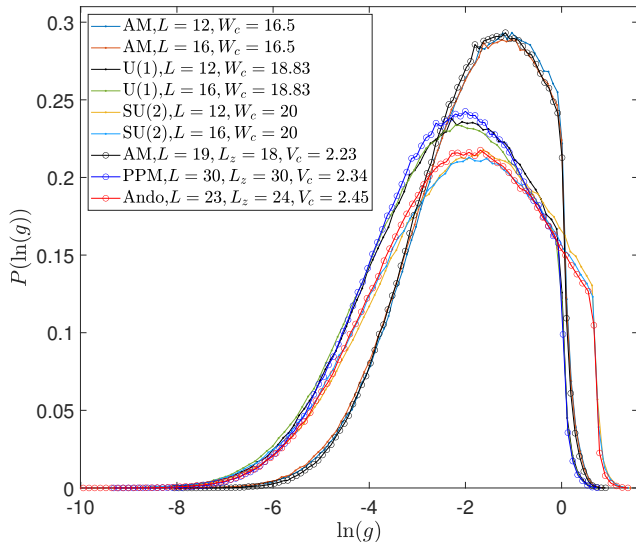


FIG. 4. Comparison of the critical conductance distributions (CCDs) between quasiperiodic and disordered systems. The lines with points stand for the CCDs of disordered systems at critical disorder  $W_c$ , i.e., Anderson model (AM), U(1) model, and SU(2) model in cubic systems with linear size  $L$ . The lines with circles are the CCDs for quasiperiodic systems at critical quasiperiodic potential  $V_c$ , i.e., AM, Peierls phase model (PPM) and Ando model, with tuned geometry (cross-section linear size  $L$  and transmission length  $L_z$ ). Data for each distribution comes from  $10^6$  samples.

## V. CRITICAL CONDUCTANCE DISTRIBUTION

To reinforce our conclusion that the universality classes in 3D quasiperiodic systems are the same as the cases in disordered systems, we have also studied the critical conductance distributions (CCDs) and compared them with those in disordered systems.

At the critical point, the correlation length will diverge and the conductance distribution will not depend on the system size  $L$ , which has been shown in Fig. 3 (a). This also indicates that the estimates of critical points are correct.

The CCDs along  $x$  and  $y$  directions are also calculated for the 3D AM. We notice that the CCDs along  $x$ ,  $y$ , and  $z$  directions are significantly different from each other [Fig. 3 (b)], which indicates the system is anisotropic because of the QP we use. We also find that the average conductance along  $x$ ,  $y$ , and  $z$  directions, i.e.,  $\langle g_x \rangle \approx 0.24$ ,  $\langle g_y \rangle \approx 0.47$ ,  $\langle g_z \rangle \approx 0.26$ , and the average conductance of AM with random potential  $\langle g \rangle \approx 0.3$  satisfy the relationship  $\langle g_x \rangle \langle g_y \rangle \langle g_z \rangle \approx \langle g \rangle^3$ . We note that this relation is similar to that for the quasi-1D localization length [74].

To test the universality classes of the ATs driven by QP, we compare the CCDs between disordered and quasiperiodic systems. Besides the symmetry and dimension, CCD also depends on the topology [75] (i.e., the

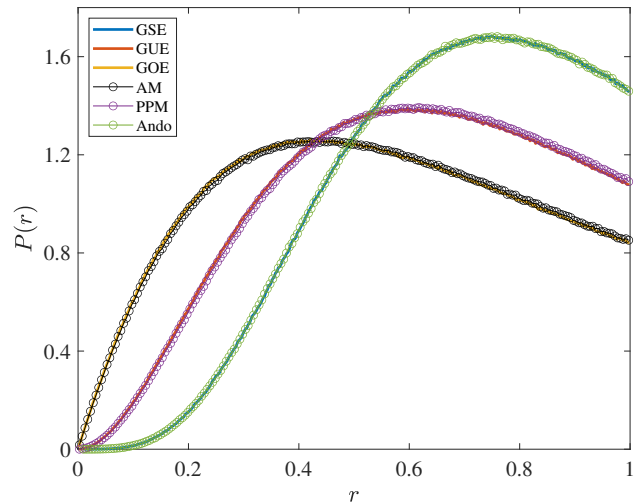


FIG. 5. Level spacing ratio distribution  $P(r)$ . The solid lines stand for the distributions of the random matrix in the Gaussian orthogonal ensemble (GOE), Gaussian unitary ensemble (GUE), and Gaussian symplectic ensemble (GSE). The circles are the distributions in the delocalized states of the Anderson model (AM), Peierls phase model (PPM), and Ando model.

boundary conditions) and effective geometry [76] (i.e., the ratio of the linear sizes between transverse direction and transmission direction, or the mean value of conductance). In order to compare the CCDs, we need to keep the symmetry, dimension, boundary condition, and effective geometry the same.

For the disordered systems, we impose the open boundary condition in the transverse direction and calculate the conductance in the cubic geometry. Anderson model, U(1) model [77], and SU(2) model [72] with random potential are chosen as the examples of Wigner-Dyson symmetry classes because of their isotropic property. We add the random potential with a box distribution  $[-W/2, W/2]$  to these models. The critical disorder  $W_c$  is believed to be independent of the boundary conditions [75] so here we just use  $W_c$  estimated in systems with periodic boundary condition for the CCD calculations.

The effective geometry in quasiperiodic systems is different from the real geometry because of the anisotropic conductance caused by the QP. Following the idea in Ref. 76, we can fine-tune the geometry ratio of these quasiperiodic models;  $\rho \equiv L/L_z$  with  $L$  the size in the transverse direction and  $L_z$  the transmission length, so that the mean value of conductance for quasiperiodic and isotropic disordered systems is almost the same. The ratios are set as  $\rho = 19/18$ , 1, and  $23/24$ , for the AM, PPM, and Ando model, respectively. Fig. 4 shows that CCDs of quasiperiodic and disordered systems are almost similar, which again indicates that the universality classes of the ATs in quasiperiodic and disordered systems are the same.



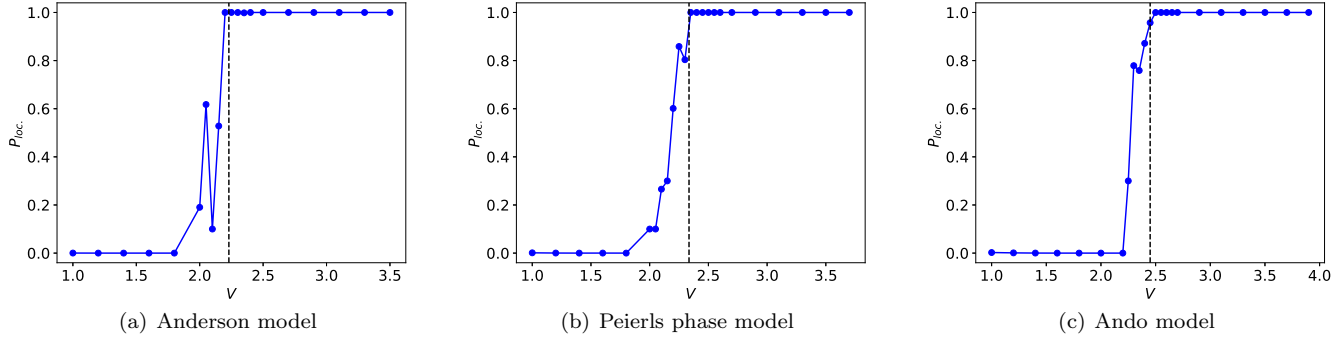


FIG. 6. The probability of localization  $P_{loc}$ , for wavefunctions in quasiperiodic systems as a function of quasiperiodic potential strength  $V$  predicted by a convolutional neural network trained by the localized/delocalized wavefunctions in the disordered Anderson model. The critical points  $V_c$  estimated in Table I are indicated by the vertical dashed lines as a guide to the eye. The probability of each data point is averaged by 10 samples. One wavefunction is selected near  $E = 0$  in a cubic system with linear size  $L = 42$  for each sample with random  $\{\phi_i\}$ .

## VI. LEVEL SPACING RATIO DISTRIBUTION

The level spacing ratio has been introduced to characterize the energy level repulsion in Ref. 78. Let  $\{E_i\}$  be a series of energy levels indexed in ascending order and  $s_i = E_i - E_{i-1}$  is the nearest-neighbor spacing. Then the level spacing ratio is defined as

$$r_i \equiv \frac{\min\{s_i, s_{i-1}\}}{\max\{s_i, s_{i-1}\}}. \quad (13)$$

According to the Wigner-Dyson random matrix theory [46–48], the level spacing ratio distribution  $P(r)$  follows the Wigner-like surmises for all the three random matrix ensembles [59], i.e., Gaussian orthogonal ensemble (GOE), Gaussian unitary ensemble (GUE), and Gaussian symplectic ensemble (GSE).  $P(r)$  in the delocalized states of the 1D AAH model doesn't follow the distribution of GOE [57, 58]. On the other hand,  $P(r)$  for the non-interacting Hamiltonians defined on the 2D quasiperiodic Ammann-Beenker tiling [79], 2D Moiré lattice [19], and 3D generalized AAH model [17] show the distribution expected from GOE.

Here we study the level spacing ratio distribution in the three quasiperiodic models. We diagonalize the Hamiltonian in a cubic system with linear size  $L = 10$ . We set  $V = 0.5$  for the three models and take half of the eigenenergy near  $E = 0$  so that all of the states are delocalized (see Fig. 1).  $6 \times 10^4$  samples with random phase  $\{\phi_i\}$  have been simulated for the distribution. We observe that  $P(r)$  in the delocalized states of the AM, PPM, and Ando model well coincide with the distributions of GOE, GUE, and GSE, respectively (Fig. 5).

## VII. CONVOLUTIONAL NEURAL NETWORK STUDY OF THE WAVEFUNCTION

Deep neural networks have been trained to predict the delocalization/localization probability and topological/non-topological probability of the wavefunctions in the 2D [80] and 3D [81, 82] disordered systems. Here we use a convolutional neural network (CNN) whose parameters have been trained by the localized/delocalized wavefunctions in the 3D disordered Anderson model. The details of the network structure is found in Ref. [60]. We input the wavefunctions of quasiperiodic systems at  $E = 0$  to this CNN, and let it determines the localization/delocalization probability. The predicted critical points (Fig. 6) well coincide with those estimated by conductance, which means that the localization behavior in 3D QP systems is similar to the ones in random systems.

## VIII. SUMMARY AND CONCLUDING REMARKS

In this paper, we have used three models in the 3D Wigner-Dyson symmetry classes to study the critical behavior of the ATs driven by QP. The two-terminal conductance and localization length have been calculated by the transfer matrix method. We find there is a correlation between samples, which results in the wrong estimation of their statistical errors. By carefully taking account of the statistical independence of samples, the critical exponents  $\nu$  and critical points  $V_c$  have been estimated by the finite size scaling analysis of two-terminal conductance. The estimated critical exponents  $\nu$  coincide with those of the ATs driven by random potential with the same symmetries. Our estimations of  $\nu$  for the AM and Ando model are consistent with those reported in Ref. 17 and 18. Moreover, the critical conductance distribution

and the level spacing distribution have also been studied. We also find that a convolutional neural network trained by the localized/delocalized wavefunctions in a disordered system can determine whether the wavefunctions in quasiperiodic systems are localized or not. These numerical results strongly support that the universality classes of ATs driven by QP and random potential are the same in the 3D Wigner-Dyson symmetry classes.

Considering the recent works about the universality classes of the Anderson transitions in non-Hermitian disordered systems [83–86], we can also extend the present work to check the universality classes in the non-Hermitian systems with QP, which is an interesting topic left for the future.

## ACKNOWLEDGMENTS

X. L. was supported by National Natural Science Foundation of China (Grants No.12105253 and 11934020) and the Project supported by CAEP Foundation (Grant No. CX20210035). T. O. was supported by JSPS KAKENHI Grants No. 19H00658 and 22H05114.

## Appendix A: Autocorrelation

To test whether a series of data is correlated or not, let us review how the autocorrelation is defined and calculated. Suppose there is a series of data sorted by time  $t$ , i.e.,  $\{y_t\}$  with  $t = 1, 2, \dots, T$ . The autocorrelation measures the correlation between  $y_t$  and  $y_{t+k}$  with  $k = 0, 1, 2, \dots, K$ . According to Ref. 87, the autocorrelation for lag  $k$  is defined as

$$r_k \equiv \frac{c_k}{c_0}, \quad (\text{A1})$$

where

$$c_k \equiv \frac{1}{T} \sum_{t=1}^{T-k} (y_t - \langle y \rangle)(y_{t+k} - \langle y \rangle). \quad (\text{A2})$$

$\langle \cdot \rangle$  stands for the mean value in statistics and  $c_0$  is the sample variance of the time series.

Suppose that  $q$  is the lag beyond which the theoretical autocorrelation is effectively zero. Then, according to Ref. 87, the estimated standard error of the autocorrelation at lag  $k > q$  is

$$\sigma_{r_k} = \sqrt{\frac{1}{T} \left( 1 + \sum_{j=1}^q r_j^2 \right)}. \quad (\text{A3})$$

If the series is completely random, then the standard error reduces to  $1/\sqrt{T}$ . Two standard error limits determine the 95% confidence interval under the assumption that the series is completely random. If all of the autocorrelation for lag  $k > 0$  is within the 95% confidence

interval, then we can accept the assumption, otherwise, we should reject the assumption.

In this paper, the time is replaced with the sample index, and the time  $T$  will be replaced by the number of samples  $N$ .

## Appendix B: Autocorrelation of conductance

The conductance has been averaged by  $N$  samples with random phase  $\{\phi_i\}$ ;

$$\langle g \rangle \equiv \frac{1}{N} \sum_i^N g_i. \quad (\text{B1})$$

Then the standard error of  $\langle g \rangle$  has been estimated as follows,

$$\sigma_{\langle g \rangle} = \frac{\sigma_g}{\sqrt{N}}, \quad (\text{B2})$$

where  $\sigma_g$  is the standard deviation for the single sample,

$$\sigma_g = \sqrt{\frac{\sum_{i=1}^N (g_i - \langle g \rangle)^2}{N - 1}}. \quad (\text{B3})$$

Eq. (B2) is correct when each  $g_i$  is independent and obeys the same probability distribution. However, in the quasiperiodic systems of this paper, the conductance will be almost the same when the two sets of  $\{\phi_i\}$  are close to each other. Then it would produce the correlation between the conductance when  $\{\phi_i\}$ 's are close to each other. We use  $\{\delta_{\phi_i}\}$  to characterize the distance between  $\{\phi_i\}$  and its nearest neighbor.  $\{\delta_{\phi_i}\}$  should be large enough to guarantee there is no correlation between samples. The allowed minimum distance is labeled as  $\delta_\phi$ . In the actual calculations, we simulate  $N$  samples in the space of  $\phi_1 - \phi_2 - \phi_3$  with  $\phi_i \in [0, 2\pi)$ ,  $i = 1, 2, 3$ , then the allowed simulated samples satisfy

$$N < (2\pi/\delta_\phi)^3. \quad (\text{B4})$$

In order to estimate  $\delta_\phi$ , we check the correlation of conductance with  $\{\phi_i\}$  in a linear line in the space of  $\phi_1 - \phi_2 - \phi_3$ . For example, we fix  $\phi_1$  and  $\phi_2$ , and change  $\phi_3$ . Then the conductance  $g$  is a continuous function of  $\phi_3$ , which varies smoothly within  $\delta_\phi$ . We use the autocorrelation introduced in Appendix A to test whether there is any correlation. From Fig. 7 (a)-(d), it is safe to say there is no correlation when  $\delta_\phi = 0.04\pi$ . However, the correlation is obvious when  $\delta_\phi = 0.01\pi$  [Fig. 7 (e)-(h)]. Then the allowed number of samples should satisfy  $N < 1.25 \times 10^5$ . We, therefore, chose  $N = 50000$  for the AM. We also checked the  $\delta_\phi$  for the PPM and Ando model and found that the number of samples set in this paper satisfies Eq. (B4).



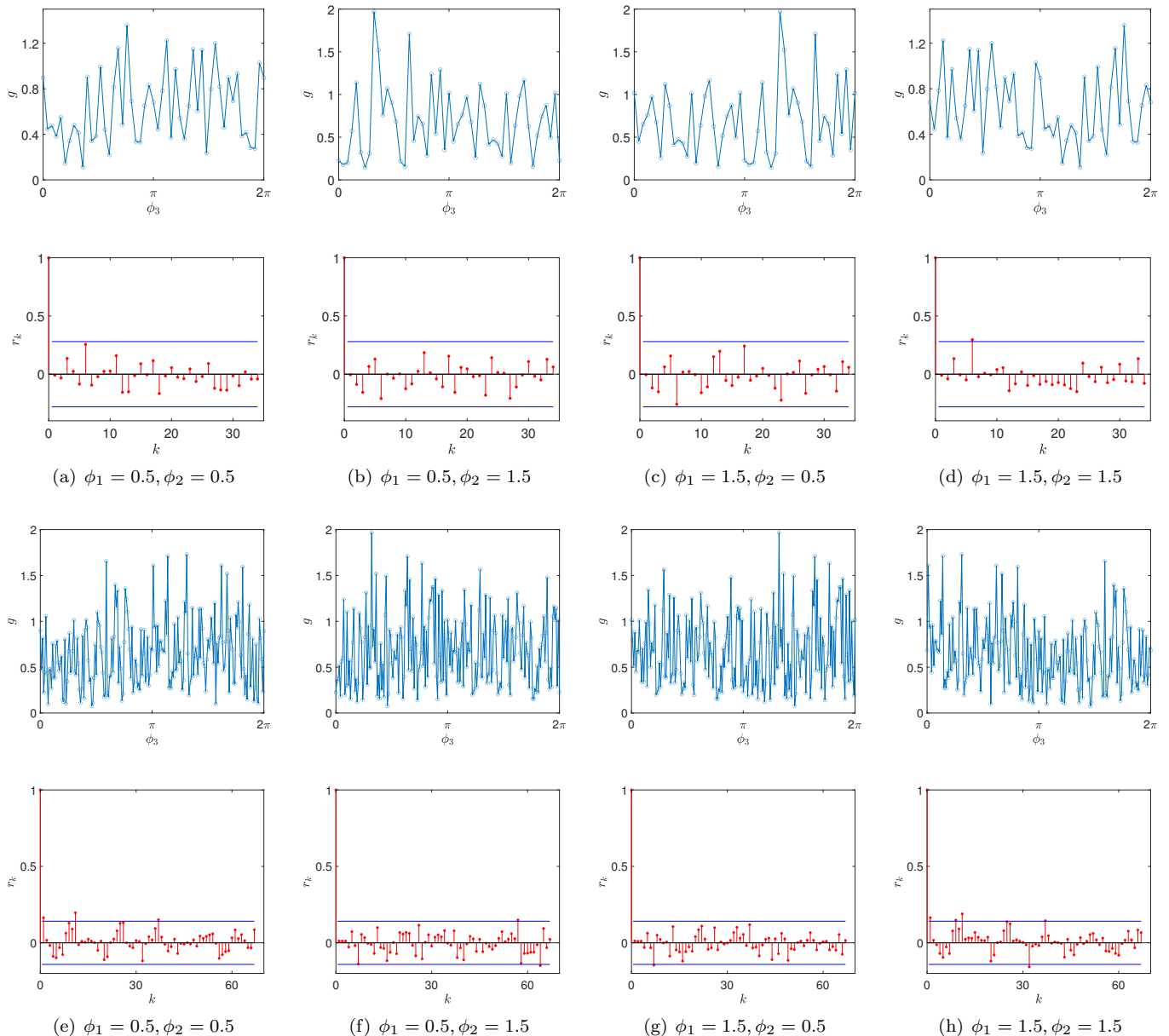


FIG. 7. The upper panel of (a)-(h): the conductance as a function of  $\phi_3$  with  $\phi_3$  changed from zero to  $2\pi$  with the interval  $\delta_\phi = 0.04\pi$  for (a)-(d), and  $\delta_\phi = 0.01\pi$  for (e)-(h).  $\phi_1$  and  $\phi_2$  are fixed. The conductance is calculated along the  $z$  direction for the Anderson model with quasiperiodic potential strength  $V = 2$  in the cubic system  $L_x = L_y = L_z = 20$ . The lower panel of (a)-(h): the autocorrelation  $r_k$  as a function of lag  $k$  for the conductance in the upper panel. The red-filled circles are the autocorrelation and the two blue lines are the two standard error limits indicating the 95% confidence interval under the assumption that the series is completely random.

### Appendix C: Autocorrelation of Lyapunov exponent

The localization length  $\lambda \equiv 1/\gamma$  with  $\gamma$  the Lyapunov exponent is also a good quantity to characterize the Anderson transition. However, we find there is also a problem with the error estimation because of the long-range correlation of QP.

Let us first review the method to estimate the error of the Lyapunov exponent [56]. We focus on the wavefunc-

tion decay in a quasi-1D system with  $L_x = L_y = L \ll L_z$ . The localization length is the slowest decay of the amplitude of wavefunction and is related to the smallest positive Lyapunov exponent  $\gamma$  by  $\lambda \equiv 1/\gamma$ . In practice, we do the  $QR$  decomposition every  $q$  layer of multiplications of the transfer matrix. We treat  $p$  ( $= n \times q$  with  $n$  integer) layers as a statistics independent sample, and the  $i$ th sample gives the estimated smallest positive Lyapunov exponent  $\gamma_i$ . Then the smallest positive Lyapunov

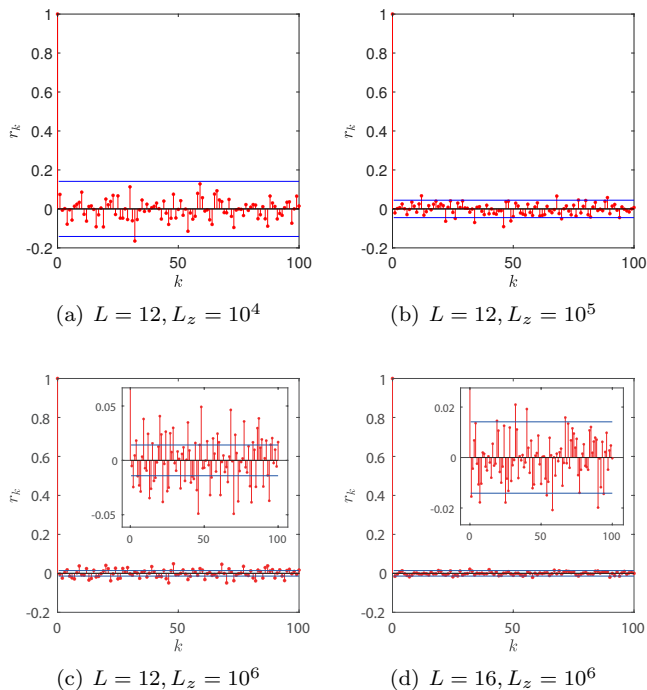


FIG. 8. The autocorrelation  $r_k$  as a function of lag  $k$  for the consecutive series of  $\{\gamma_i\}$  in the quasi-1D Anderson model with cross-section size  $L$  and transmission length  $L_z$ . The red-filled circles are the autocorrelations and the two blue lines are the two standard error limits determines the 95% confidence interval under the assumption that the series is completely random. Insets in (c) and (d): the enlarged pictures to show the detail except  $r_0 = 1$ .

exponent is estimated as

$$\gamma = \frac{1}{N} \sum_i^N \gamma_i \quad (\text{C1})$$

with  $N = L_z/p$ . Then their sample standard deviation is estimated as,

$$\sigma = \sqrt{\frac{\sum_{i=1}^N (\gamma_i - \gamma)^2}{N - 1}} \quad (\text{C2})$$

and the standard deviation of  $\gamma$  is estimated as,

$$\sigma_\gamma = \frac{\sigma}{\sqrt{N}}. \quad (\text{C3})$$

Similar to the conductance,  $\{\gamma_i\}$  should be independent and without correlations in order to estimate  $\sigma_\gamma$  correctly according to Eq. (C3). However, we find there are correlations for  $\{\gamma_i\}$  in our quasiperiodic systems. We use the autocorrelation introduced in Appendix A to test the correlation of a series of  $\{\gamma_i\}$ . We just take the AM with QP as an example and set  $V = 2$  and  $p = 50$ . In Fig. 8 (a)-(c), the autocorrelation for cross-section size  $L = 12$  have a tendency to go beyond the 95% confidence interval with increasing the transmission length  $L_z$ , which suggests the correlation would be strong for  $\{\gamma_i\}$  with larger  $L_z$ . This means  $L_z$  should be small if we want to guarantee that there is no correlation. However, to extract the critical exponent precisely from localization length, the transmission length  $L_z$  should be large enough, such as  $10^7$ . Then the correlation of the Lyapunov exponent will limit the precise estimations of the critical exponents in quasiperiodic systems. We also note that a larger cross-section size  $L = 16$  could reduce the correlation [Fig. 8(d)], but the cost of computation will increase as  $L^7$ .

- 
- [1] P. W. Anderson, Absence of Diffusion in Certain Random Lattices, *Phys. Rev.* **109**, 1492 (1958).
- [2] E. Abrahams, P. W. Anderson, D. C. Licciardello, and T. V. Ramakrishnan, Scaling Theory of Localization: Absence of Quantum Diffusion in Two Dimensions, *Phys. Rev. Lett.* **42**, 673 (1979).
- [3] F. Evers and A. D. Mirlin, Anderson transitions, *Rev. Mod. Phys.* **80**, 1355 (2008).
- [4] S. Aubry and G. André, Analyticity breaking and Anderson localization in incommensurate lattices, in *Group theoretical methods in physics (Proc. Eighth Internat. Colloq., Kiryat Anavim, 1979)*, Ann. Israel Phys. Soc., Vol. 3 (Hilger, Bristol, 1980) pp. 133–164.
- [5] J. B. Sokoloff, Electron localization in crystals with quasiperiodic lattice potentials, *Phys. Rev. B* **22**, 5823 (1980).
- [6] I. M. Suslov, Localization in one-dimensional incommensurate systems, *Zh. Eksp. Teor. Fiz.* **83**, 1079 (1982).
- [7] M. Kohmoto, Metal-Insulator Transition and Scaling for Incommensurate Systems, *Phys. Rev. Lett.* **51**, 1198 (1983).
- [8] C. M. Soukoulis and E. N. Economou, Localization in One-Dimensional Lattices in the Presence of Incommensurate Potentials, *Phys. Rev. Lett.* **48**, 1043 (1982).
- [9] S. Das Sarma, S. He, and X. C. Xie, Mobility Edge in a Model One-Dimensional Potential, *Phys. Rev. Lett.* **61**, 2144 (1988).
- [10] J. Biddle and S. Das Sarma, Predicted Mobility Edges in One-Dimensional Incommensurate Optical Lattices: An Exactly Solvable Model of Anderson Localization, *Phys. Rev. Lett.* **104**, 070601 (2010).
- [11] H. Yao, A. Khoudli, L. Bresque, and L. Sanchez-Palencia, Critical Behavior and Fractality in Shallow One-Dimensional Quasiperiodic Potentials, *Phys. Rev. Lett.* **123**, 070405 (2019).
- [12] S. Ganeshan, J. H. Pixley, and S. Das Sarma, Nearest Neighbor Tight Binding Models with an Exact Mobility Edge in One Dimension, *Phys. Rev. Lett.* **114**, 146601

- (2015).
- [13] S. Roy, T. Mishra, B. Tanatar, and S. Basu, Reentrant Localization Transition in a Quasiperiodic Chain, *Phys. Rev. Lett.* **126**, 106803 (2021).
- [14] L. Sanchez-Palencia and L. Santos, Bose-Einstein condensates in optical quasicrystal lattices, *Phys. Rev. A* **72**, 053607 (2005).
- [15] A.-M. Guo, X. C. Xie, and Q.-f. Sun, Delocalization and scaling properties of low-dimensional quasiperiodic systems, *Phys. Rev. B* **89**, 075434 (2014).
- [16] M. Rossignolo and L. Dell'Anna, Localization transitions and mobility edges in coupled Aubry-André chains, *Phys. Rev. B* **99**, 054211 (2019).
- [17] T. Devakul and D. A. Huse, Anderson localization transitions with and without random potentials, *Phys. Rev. B* **96**, 214201 (2017).
- [18] J. Sutrardhar, S. Mukerjee, R. Pandit, and S. Banerjee, Transport, multifractality, and the breakdown of single-parameter scaling at the localization transition in quasiperiodic systems, *Phys. Rev. B* **99**, 224204 (2019).
- [19] B. Huang and W. V. Liu, Moiré localization in two-dimensional quasiperiodic systems, *Phys. Rev. B* **100**, 144202 (2019).
- [20] A. Szabó and U. Schneider, Mixed spectra and partially extended states in a two-dimensional quasiperiodic model, *Phys. Rev. B* **101**, 014205 (2020).
- [21] M. Gonçalves, H. Z. Olyaei, B. Amorim, R. Mondaini, P. Ribeiro, and E. V. Castro, Incommensurability-induced sub-ballistic narrow-band-states in twisted bilayer graphene, *2D Materials* **9**, 011001 (2021).
- [22] C. Huang, F. Ye, X. Chen, Y. V. Kartashov, V. V. Konotop, and L. Torner, Localization-delocalization wavepacket transition in pythagorean aperiodic potentials, *Sci. Rep.* **6**, 32546 (2016).
- [23] Y. Wang and S. Chen, Fate of Weyl semimetals in the presence of incommensurate potentials, *Phys. Rev. A* **95**, 053634 (2017).
- [24] J. H. Pixley, J. H. Wilson, D. A. Huse, and S. Gopalakrishnan, Weyl Semimetal to Metal Phase Transitions Driven by Quasiperiodic Potentials, *Phys. Rev. Lett.* **120**, 207604 (2018).
- [25] Y. Lahini, R. Pugatch, F. Pozzi, M. Sorel, R. Morandotti, N. Davidson, and Y. Silberberg, Observation of a Localization Transition in Quasiperiodic Photonic Lattices, *Phys. Rev. Lett.* **103**, 013901 (2009).
- [26] M. Sbroscia, K. Viebahn, E. Carter, J.-C. Yu, A. Gaunt, and U. Schneider, Observing Localization in a 2D Quasicrystalline Optical Lattice, *Phys. Rev. Lett.* **125**, 200604 (2020).
- [27] P. Wang, Y. Zheng, X. Chen, C. Huang, Y. V. Kartashov, L. Torner, V. V. Konotop, and F. Ye, Localization and delocalization of light in photonic moiré lattices, *Nature* **577**, 42 (2020).
- [28] G. Roati, C. D'Errico, L. Fallani, M. Fattori, C. Fort, M. Zaccanti, G. Modugno, M. Modugno, and M. Inguscio, Anderson localization of a non-interacting Bose-Einstein condensate, *Nature* **453**, 895 (2008).
- [29] M. Lopez, J. F. Clement, P. Szriftgiser, J. C. Garreau, and D. Delande, Experimental Test of Universality of the Anderson Transition, *Phys. Rev. Lett.* **108**, 095701 (2012).
- [30] H. P. Lüschen, S. Scherg, T. Kohlert, M. Schreiber, P. Bordia, X. Li, S. Das Sarma, and I. Bloch, Single-Particle Mobility Edge in a One-Dimensional Quasiperiodic Optical Lattice, *Phys. Rev. Lett.* **120**, 160404 (2018).
- [31] V. Goblot, A. Štrkalj, N. Pernet, J. L. Lado, C. Dorow, A. Lemaître, L. Le Gratiet, A. Harouri, I. Sagnes, S. Ravets, A. Amo, J. Bloch, and O. Zilberberg, Emergence of criticality through a cascade of delocalization transitions in quasiperiodic chains, *Nature Physics* **16**, 832 (2020).
- [32] F. A. An, K. Padavić, E. J. Meier, S. Hegde, S. Ganeshan, J. H. Pixley, S. Vishveshwara, and B. Gadway, Interactions and Mobility Edges: Observing the Generalized Aubry-André Model, *Phys. Rev. Lett.* **126**, 040603 (2021).
- [33] D. Shechtman, I. Blech, D. Gratias, and J. W. Cahn, Metallic Phase with Long-Range Orientational Order and No Translational Symmetry, *Phys. Rev. Lett.* **53**, 1951 (1984).
- [34] M. Schreiber, S. S. Hodgman, P. Bordia, H. P. Lüschen, M. H. Fischer, R. Vosk, E. Altman, U. Schneider, and I. Bloch, Observation of many-body localization of interacting fermions in a quasirandom optical lattice, *Science* **349**, 842 (2015).
- [35] P. Bordia, H. Lüschen, U. Schneider, M. Knap, and I. Bloch, Periodically driving a many-body localized quantum system, *Nature Physics* **13**, 460 (2017).
- [36] B. Deissler, M. Zaccanti, G. Roati, C. D'Errico, M. Fattori, M. Modugno, G. Modugno, and M. Inguscio, Delocalization of a disordered bosonic system by repulsive interactions, *Nature Physics* **6**, 354 (2010).
- [37] S. Nakajima, N. Takei, K. Sakuma, Y. Kuno, P. Marra, and Y. Takahashi, Competition and interplay between topology and quasi-periodic disorder in Thouless pumping of ultracold atoms, *Nature Physics* **17**, 844-849 (2021).
- [38] R. Bistritzer and A. H. MacDonald, Moiré bands in twisted double-layer graphene, *Proceedings of the National Academy of Sciences* **108**, 12233 (2011).
- [39] W. Yao, E. Wang, C. Bao, Y. Zhang, K. Zhang, K. Bao, C. K. Chan, C. Chen, J. Avila, M. C. Asensio, J. Zhu, and S. Zhou, Quasicrystalline 30° twisted bilayer graphene as an incommensurate superlattice with strong interlayer coupling, *Proceedings of the National Academy of Sciences* **115**, 6928 (2018).
- [40] P. G. Harper, Single band motion of conduction electrons in a uniform magnetic field, *Proceedings of the Physical Society. Section A* **68**, 874 (1955).
- [41] D. R. Hofstadter, Energy levels and wave functions of Bloch electrons in rational and irrational magnetic fields, *Phys. Rev. B* **14**, 2239 (1976).
- [42] Y. E. Kraus, Y. Lahini, Z. Ringel, M. Verbin, and O. Zilberberg, Topological States and Adiabatic Pumping in Quasicrystals, *Phys. Rev. Lett.* **109**, 106402 (2012).
- [43] Y. E. Kraus, Z. Ringel, and O. Zilberberg, Four-Dimensional Quantum Hall Effect in a Two-Dimensional Quasicrystal, *Phys. Rev. Lett.* **111**, 226401 (2013).
- [44] M. Verbin, O. Zilberberg, Y. E. Kraus, Y. Lahini, and Y. Silberberg, Observation of Topological Phase Transitions in Photonic Quasicrystals, *Phys. Rev. Lett.* **110**, 076403 (2013).
- [45] O. Zilberberg, S. Huang, J. Guglielmon, M. Wang, K. P. Chen, Y. E. Kraus, and M. C. Rechtsman, Photonic topological boundary pumping as a probe of 4D quantum Hall physics, *Nature* **553**, 59 (2018).
- [46] E. P. Wigner, On the statistical distribution of the widths

- and spacings of nuclear resonance levels, *Mathematical Proceedings of the Cambridge Philosophical Society* **47**, 790–798 (1951).
- [47] F. J. Dyson, Statistical theory of the energy levels of complex systems. I, *Journal of Mathematical Physics* **3**, 140 (1962).
- [48] F. J. Dyson, Threefold Way - Algebraic Structure of Symmetry Groups and Ensembles in Quantum Mechanics, *Journal of Mathematical Physics* **3**, 1199 (1962).
- [49] R. Peierls, Zur theorie des diamagnetismus von leitungsselektronen, *Zeitschrift für Physik* **80**, 763 (1933).
- [50] J. M. Luttinger, The Effect of a Magnetic Field on Electrons in a Periodic Potential, *Phys. Rev.* **84**, 814 (1951).
- [51] T. Ando, Numerical study of symmetry effects on localization in two dimensions, *Phys. Rev. B* **40**, 5325 (1989).
- [52] T. Kawarabayashi, T. Ohtsuki, K. Slevin, and Y. Ono, Anderson Transition in Three-Dimensional Disordered Systems with Symplectic Symmetry, *Phys. Rev. Lett.* **77**, 3593 (1996).
- [53] J. L. Pichard and G. Sarma, Finite size scaling approach to Anderson localisation, *Journal of Physics C: Solid State Physics* **14**, L127 (1981).
- [54] A. MacKinnon and B. Kramer, The scaling theory of electrons in disordered solids: Additional numerical results, *Zeitschrift für Physik B Condensed Matter* **53**, 1 (1983).
- [55] A. MacKinnon, Critical exponents for the metal-insulator transition, *Journal of Physics: Condensed Matter* **6**, 2511 (1994).
- [56] K. Slevin and T. Ohtsuki, Critical exponent for the Anderson transition in the three-dimensional orthogonal universality class, *New Journal of Physics* **16**, 015012 (2014).
- [57] X. Li, J. H. Pixley, D.-L. Deng, S. Ganeshan, and S. Das Sarma, Quantum nonergodicity and fermion localization in a system with a single-particle mobility edge, *Phys. Rev. B* **93**, 184204 (2016).
- [58] D.-L. Deng, S. Ganeshan, X. Li, R. Modak, S. Mukerjee, and J. H. Pixley, Many-body localization in incommensurate models with a mobility edge, *Annalen der Physik* **529**, 1600399 (2017).
- [59] Y. Y. Atas, E. Bogomolny, O. Giraud, and G. Roux, Distribution of the Ratio of Consecutive Level Spacings in Random Matrix Ensembles, *Phys. Rev. Lett.* **110**, 084101 (2013).
- [60] T. Ohtsuki and T. Mano, Drawing phase diagrams of random quantum systems by deep learning the wave functions, *Journal of the Physical Society of Japan* **89**, 022001 (2020).
- [61] X. Li, X. Li, and S. Das Sarma, Mobility edges in one-dimensional bichromatic incommensurate potentials, *Phys. Rev. B* **96**, 085119 (2017).
- [62] X. Li and S. Das Sarma, Mobility edge and intermediate phase in one-dimensional incommensurate lattice potentials, *Phys. Rev. B* **101**, 064203 (2020).
- [63] J. B. Pendry, A. MacKinnon, and P. J. Roberts, Universality classes and fluctuations in disordered systems, *Proceedings of the Royal Society of London. Series A: Mathematical and Physical Sciences* **437**, 67 (1992).
- [64] C. P. Umbach, S. Washburn, R. B. Laibowitz, and R. A. Webb, Magnetoresistance of small, quasi-one-dimensional, normal-metal rings and lines, *Phys. Rev. B* **30**, 4048 (1984).
- [65] A. D. Stone, Magnetoresistance Fluctuations in Mesoscopic Wires and Rings, *Phys. Rev. Lett.* **54**, 2692 (1985).
- [66] R. A. Webb, S. Washburn, C. P. Umbach, and R. B. Laibowitz, Observation of  $\frac{h}{e}$  Aharonov-Bohm Oscillations in Normal-Metal Rings, *Phys. Rev. Lett.* **54**, 2696 (1985).
- [67] P. A. Lee and A. D. Stone, Universal Conductance Fluctuations in Metals, *Phys. Rev. Lett.* **55**, 1622 (1985).
- [68] S. Daimon, K. Tsunekawa, S. Kawakami, T. Kikkawa, R. Ramos, K. Oyanagi, T. Ohtsuki, and E. Saitoh, Deciphering quantum fingerprints in electric conductance, *Nature Communications* **13**, 3160 (2022).
- [69] K. Slevin and T. Ohtsuki, Corrections to Scaling at the Anderson Transition, *Phys. Rev. Lett.* **82**, 382 (1999).
- [70] P. R. Bevington and D. K. Robinson, *Data Reduction and Error Analysis for the Physical Sciences* (McGraw-Hill, 2003).
- [71] W. H. Press, B. P. Flannery, S. A. Teukolsky, and W. T. Vetterling, *Numerical Recipes in FORTRAN : The Art of Scientific Computing* (Cambridge University Press, 1992).
- [72] Y. Asada, K. Slevin, and T. Ohtsuki, Anderson Transition in the Three Dimensional Symplectic Universality Class, *Journal of the Physical Society of Japan* **74**, 238 (2005).
- [73] P. A. Lee and T. V. Ramakrishnan, Disordered electronic systems, *Rev. Mod. Phys.* **57**, 287 (1985).
- [74] I. Zambetaki, Q. Li, E. N. Economou, and C. M. Soukoulis, Localization in Highly Anisotropic Systems, *Phys. Rev. Lett.* **76**, 3614 (1996).
- [75] K. Slevin, T. Ohtsuki, and T. Kawarabayashi, Topology Dependent Quantities at the Anderson Transition, *Phys. Rev. Lett.* **84**, 3915 (2000).
- [76] X. Luo, B. Xu, T. Ohtsuki, and R. Shindou, Quantum multicriticality in disordered Weyl semimetals, *Phys. Rev. B* **97**, 045129 (2018).
- [77] K. Slevin and T. Ohtsuki, Estimate of the Critical Exponent of the Anderson Transition in the Three and Four-Dimensional Unitary Universality Classes, *Journal of the Physical Society of Japan* **85**, 104712 (2016).
- [78] V. Oganesyan and D. A. Huse, Localization of interacting fermions at high temperature, *Phys. Rev. B* **75**, 155111 (2007).
- [79] U. Grimm and R. A. Römer, Gaussian orthogonal ensemble for quasiperiodic tilings without unfolding:  $r$ -value statistics, *Phys. Rev. B* **104**, L060201 (2021).
- [80] T. Ohtsuki and T. Ohtsuki, Deep learning the quantum phase transitions in random two-dimensional electron systems, *Journal of the Physical Society of Japan* **85**, 123706 (2016).
- [81] T. Ohtsuki and T. Ohtsuki, Deep learning the quantum phase transitions in random electron systems: Applications to three dimensions, *Journal of the Physical Society of Japan* **86**, 044708 (2017).
- [82] T. Mano and T. Ohtsuki, Phase Diagrams of Three-Dimensional Anderson and Quantum Percolation Models Using Deep Three-Dimensional Convolutional Neural Network, *Journal of the Physical Society of Japan* **86**, 113704 (2017).
- [83] Y. Huang and B. I. Shklovskii, Anderson transition in three-dimensional systems with non-Hermitian disorder, *Phys. Rev. B* **101**, 014204 (2020).
- [84] X. Luo, T. Ohtsuki, and R. Shindou, Universality Classes of the Anderson Transitions Driven by Non-Hermitian Disorder, *Phys. Rev. Lett.* **126**, 090402 (2021).
- [85] X. Luo, T. Ohtsuki, and R. Shindou, Transfer matrix study of the Anderson transition in non-Hermitian sys-

- tems, Phys. Rev. B **104**, 104203 (2021).
- [86] X. Luo, Z. Xiao, K. Kawabata, T. Ohtsuki, and R. Shindou, Unifying the Anderson transitions in Hermitian and non-Hermitian systems, Phys. Rev. Research **4**, L022035 (2022).
- [87] J. D. Hamilton, *Time Series Analysis* (Princeton University Press, 1994).